Kinetics of a Gas-Phase Chain Reaction Catalyzed by a Solid: The Oxidative Coupling of Methane over Li/MgO-Based Catalysts

Pieter M. Couwenberg,[†] Qi Chen,[‡] and Guy B. Marin*

Laboratorium voor Chemische Technologie, Eindhoven University of Technology, P.O. Box 513, 5600 MB Eindhoven, The Netherlands

A kinetic model was developed for the heterogeneously catalyzed oxidative coupling of methane for temperatures between 923 and 1023 K, inlet methane-to-oxygen ratios of 2 to 12, and oxygen conversions between 10 and 100%. This model features 10 catalytic reactions coupled to 39 gas-phase chain reactions and accounts for irreducible mass-transport limitations for reactive intermediates. The observed conversions and selectivities are adequately described up to 200 kPa total pressure. The observed strong increase of the conversions between 200 and 1000 kPa is described qualitatively. The catalyst not only produces radicals but also acts as an important radical quencher. Regeneration of the active sites through water desorption was found to be a kinetically significant step in the catalytic sequence producing methyl radicals. At atmospheric pressure approximately 90% of the methane and oxygen is converted on the surface of Sn/Li/MgO, the balance being converted through branched-chain reactions in the pores of the catalyst and in the interstitial phase. For Li/MgO only one-third of the methane is converted on the catalyst surface. For Sn/Li/MgO the catalytic oxidation of methyl radicals, rather than gas-phase reactions, limits the selectivity toward C_2 products.

Introduction

In recent years a lot of research on the oxidative coupling of methane was performed to provide a direct route for the production of higher hydrocarbons from natural gas. The process occurs through a mechanism in which catalytic reactions interact with gas-phase chain reactions. The existence of such a mechanism was first reported by Polyakov et al. (1936) for the total oxidation of methane. Fang and Yeh (1981) studied methane pyrolysis over ThO_2/SiO_2 and proposed a reaction mechanism consisting of methyl-radical formation on the catalyst surface and subsequent coupling of these radicals in the gas phase to produce ethane.

A wide variety of catalysts has been tested but the lithium-doped magnesium oxide, which was first reported by Ito et al. in 1985, is still among the best catalysts mentioned in open literature. The highest yield on a Li/MgO catalyst amounts to 18.7% for undiluted feed gases (Ekström et al., 1990). Some kinetic and mechanistic studies on lithium magnesia catalysts were published (Roos et al., 1989, Aparicio et al., 1991; Tung and Lobban, 1992). Roos et al. (1989) derived rate equations for methane consumption and regressed these on experimental data obtained in a gradientless reactor. Tung and Lobban (1992) also derived rate equations for the production of C_2 products and CO_2 based on a four-step reaction mechanism. The first study combining catalytic reactions and a few important gas-phase reactions was presented by Aparicio et al. (1991). Other kinetic studies on various catalysts in which gas-phase reactions are coupled to catalytic reactions were performed by Zanthoff and Baerns (1992), Bistolfi et al. (1992), McCarty (1992), and Reyes et al. (1993).

Couwenberg et al. (1996) addressed a feature characteristic for such heterogeneous−homogeneous reaction mechanisms, i.e., the existence of irreducible mass-transport limitations for the reactive intermediates even in the absence of mass-transport limitations for the reactants and the products. These limitations were called irreducible because the pellet size at which they would be negligible is much smaller than the minimum pellet size allowed for pressure drop considerations. Irreducible mass-transport limitations are well-known (Boudart, 1968), e.g., in polymerization reactions and chain reactions in the gas phase. Because these irreducible mass-transport limitations were shown to have significant effects on the coupling selectivity, a method to take these limitations into account quantitatively during a kinetic study was developed. The latter consists of regressing the experimental data with heterogeneous reactor model equations in which a distinction is made between the interstitial gas phase, i.e., in between the catalyst pellets, and the intraparticle phase. External mass transfer by molecular diffusion with simultaneous gas-phase reactions and internal diffusion with simultaneous reactions on the catalyst surface and in the pores of the catalyst is explicitly accounted for during the data analysis.

The present work reports on the development of a kinetic model for a lithium on magnesium oxide catalyst either tin promoted or not, including the irreducible transport limitations. The kinetic model consists of elementary catalytic reactions coupled to the gas-phase reaction network reported by Chen et al. (1994b). The considered catalytic reactions are based on kinetic experiments and on information provided by pulse experiments performed on a TAP setup (Gleaves et al., 1988; Mallens et al., 1995) and steady-state transient isotopic kinetic (SSTIKA) experiments (Nibbelke et al. 1995) on the same catalyst.

The developed kinetic model provides insights in the important steps in the reaction mechanism, in particular the interplay of the gas-phase chain reactions with the catalytic reactions, and in the importance of mass transport herein.

* To whom correspondence should be addressed.

[†] Present address: AspenTech Europe b.v., Best Office, de Waal 32, 5684PH, Best, The Netherlands.

[‡] Present address: KTI, P.O. Box 86, 2700 AB Zoetermeer, The Netherlands.

S0888-5885(95)00461-1 CCC: $12.00

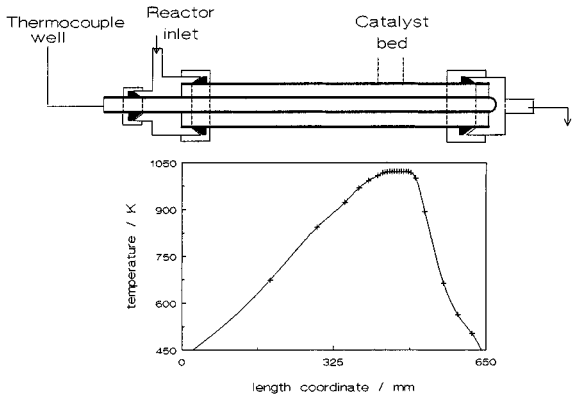

Figure 1. Experimental reactor and a typical axial temperature profile.

Experimental Section

Reactor. The setup used for the kinetic experiments in this study has been described previously by Chen et al. (1994a) for the measurement of the kinetics in the absence of catalyst. For the present study a continuous-flow, sintered α-Al_2O_3 tubular reactor with a length of 650 mm, an external diameter of 12 mm, and an internal diameter of 8 mm was used. In the centerline of the reactor an α-Al_2O_3 thermocouple well with an external diameter of 4 mm is placed, allowing the measurement of the axial temperature profile. The reactor was heated with a fluidized-sand bed in order to achieve a uniform outside wall temperature. A typical axial temperature profile is shown in Figure 1. During the experiments the catalyst bed was placed in the flat part of the temperature profile. To reduce the volume of the postcatalytic space, an α-Al_2O_3 tube was fixed in the bottom part of the reactor using a ceramic kit. Quartz wool serving as a support filter was placed on this inner tube, and hereon a layer of α-Al_2O_3 pellets was placed. The catalyst bed diluted with inert α-Al_2O_3 pellets was poured on this layer.

Some alumina particles were put on the catalyst bed on which a removable tube was placed to reduce the volume of the precatalytic space. A lot of attention was payed to make sure that the reactor was operated in the plug-flow regime, without disturbing axial and radial temperature gradients, and a negligible pressure drop over the catalyst bed. To prevent significant radial temperature gradients, the catalyst bed was diluted with inert α-Al_2O_3 pellets in a ratio of 7 $vol_{diluent}/vol_{catalyst}$ (Mears, 1971).

Reactor Model. The heterogeneously catalyzed oxidative coupling of methane occurs through a mechanism in which the catalyst produces radicals which react further through gas-phase branched-chain reactions in the pores of the catalyst and in the void space between the catalyst pellets. Couwenberg et al. (1996) showed that because of the very high reactivity of the surface-produced radicals irreducible mass-transport limitations occur for these species even when no concentration gradients develop for the stable components, i.e., the reactants and the products. Furthermore, it was shown that these irreducible mass-transport limitations have an important effect on the selectivity of the process. Therefore, during the simulation of the kinetic experiments these limitations have to be taken into account by use of a heterogeneous reactor model. Couwenberg et al. (1996) developed a one-dimensional heterogeneous model distinguishing between the interstitial and intraparticle phase. Usually a film model is applied to describe mass transfer from the interstitial phase to the intraparticle phase (Froment and Bischoff, 1990). At the conditions investigated, however, the Reynolds number amounts to approximately 1.5, which is so low that the film thickness is of the same order of magnitude as the pellet radius, i.e., 1.0×10^{-4} m. Therefore, it was assumed that mass transfer from the interstitial phase to the intraparticle phase was solely a result of molecular diffusion. Because the laboratory reactor was operated in the plug-flow regime and the calculated radial temperature gradient was less than 2 K, a one-dimensional model could be used. Since the measured axial temperature gradient and pressure drop could be neglected as well, the reactor model only contains the continuity equations of all components in the kinetic network. The continuity equations in the interstitial phase describe convection in the axial direction and mass transfer from the interstitial phase to the intraparticle phase by molecular diffusion with simultaneous gas-phase reactions. The continuity equations in the intraparticle phase describe internal diffusion with simultaneous reactions on the catalyst surface and gas-phase reactions in the pores of the catalyst. Simulations with this model (Couwenberg et al., 1996) show that the concentration of the methyl radicals in the center of the catalyst pellet is approximately 5 times higher than the interstitial concentration, even when no significant concentration gradient occurs for methane and oxygen.

Since the irreducible mass-transport limitations are accounted for during the analysis of the laboratory data, intrinsic values for the kinetic parameters could be obtained. These kinetic parameters could, therefore, be applied in a straightforward way for the design of an industrial fixed-bed reactor (Hoebink et al., 1994).

Catalysts. The Li/MgO and the Sn/Li/MgO catalyst were prepared according to Korf et al. (1989). Due to the initial transient in the first couple of hours on stream, the catalysts had to be lined-out according to a standard procedure before the kinetic experiments could be started. This line-out procedure was performed in the setup used for the experiments and featured two steps. In step one the reactor is heated up under a continuous helium flow. Once the desired temperature is reached, methane is fed to the reactor, immediately followed by oxygen. Hereafter, the flow of helium is stopped. For the conditions applied during the line-out and the conversion and selectivity reached at the end of the procedure the reader is referred to Couwenberg (1996). Although the line-out temperature applied for the Sn/Li/MgO catalyst is 100 K lower than that for Li/MgO, the space time yield after line-out is considerably higher. The addition of tin made the catalyst more stable and active at low temperature and therefore allowed a lower line-out temperature. The lower line-out temperature also had a positive effect on the lifetime of the catalyst. All experiments were performed within 12 h after the line-out procedure to ensure that the measurements are not disturbed by deactivation.

Conditions. The number of kinetic experiments performed amounts to 130 for the Sn/Li/MgO catalyst and to 50 for the Li/MgO catalyst. The ranges of the experimental conditions covered are shown in Table 1 and include the range of industrially relevant operation conditions. The experimental reactor was designed such that mass-transport and mass-transfer limitations for

Table 1. Experimental Conditions Covered during the Kinetic Experiments over Li/MgO and Sn/Li/MgO (Columns 1 and 2) and during Parameter Estimation (Column 3)

	Li/MgO	Sn/Li/MgO	Sn/Li/MgO param estimation
T (K)	998−1098	923−1023	973−1023
p_t (kPa)	100−414	100−1000	110−150
$W/F_{t,0}$ (kg s mol^{-1})	4−14	0.2−12	1−10
$CH_4/O_2\|_0$ (mol mol^{-1})	2.0−10	2.0−12	2.0−12
$C_2H_6/CH_4\|_0$ (mol mol^{-1})	0	0−0.1	0−0.1
$CO_2/CH_4\|_0$ (mol mol^{-1})	0	0−0.2	0−0.2
X_{CH_4} (%)	1−19	2.6−25	2.6−15
X_{O_2} (%)	6−87	9.6−99	15−75

the reactants and the products were negligible. The way of calculating the conversions, selectivities, and yields is similar to Chen et al. (1994a).

Parameter Estimation. The kinetic parameters of the catalytic reactions were estimated using a Marquardt nonlinear multiresponse minimization algorithm (Marquardt, 1963; Froment and Hosten, 1981). In this method the maximum-likelihood parameter estimates, b, were obtained by minimization of the least-squares criterion applied on the observed, y, and calculated, $\hat{y}$, mole fractions at the reactor outlet.

$$S(b) = \sum_{h=1}^{v}\sum_{k=1}^{v}\sigma^{hk}\sum_{i=1}^{n}(y_{ih} - \hat{y}_{ih})(y_{ik} - \hat{y}_{ik}) \rightarrow \text{MIN} \qquad (1)$$

where v is the number of responses, n the number of observations, and σ^{hk} an element of the inverse of the error variance−covariance matrix. This criterion is based upon the assumption that the experimental errors are normally distributed with a zero mean. The elements σ^{hk} of the inverse of the error variance−covariance matrix are estimated by the regression routine from a regression with a unit error variance−covariance matrix. The mole fractions of methane, oxygen, carbon monoxide, carbon dioxide, ethene, and ethane at the reactor outlet were used as responses. The third column in Table 1 shows the range of experimental conditions covered during the parameter estimation. Experiments at pressures higher than 150 kPa were not taken into account because simulation of these experiments sometimes causes numerical problems. Only 24 experiments were used to reduce the CPU time needed. To simulate one experiment on a Silicon Graphics Power Challenge Computer, the required CPU time amounts to approximately 1 min. During every iteration in the Marquardt algorithm, every experiment has to be simulated at least 11 times, i.e., the number of parameters to be estimated plus 1. Every iteration thus takes at least 260 min CPU time. When good initial parameters are provided, 5−10 iterations are sufficient to reach the minimum of the objective function. The initial estimates were chosen within the range of physically realistic values (Zdanov et al., 1988; Dumesic et al., 1993) expected for the rate coefficients corresponding to the elementary steps, and dependencies between parameters were determined using physicochemical relations analogous to Aparicio et al. (1991) and Bistolfi et al. (1992).

The parameter estimates were tested for significance by means of their approximate individual t-values.

Table 2. Reactions Considered on a Sn/Li/MgO Catalyst Surface (1−10) and Corresponding Global Reaction Paths (a−e)

	σ_a	σ_b	σ_c	σ_d	σ_e	
$O_2 + 2* \rightleftharpoons 2O*$	1	1	1	1	7	(1)
$CH_4 + O* \rightarrow CH_3^{\bullet} + OH*$	4	0	0	0	0	(2)
$C_2H_6 + O* \rightarrow C_2H_5^{\bullet} + OH*$	0	4	0	0	0	(3)
$C_2H_4 + O* \rightarrow C_2H_3^{\bullet} + OH*$	0	0	4	0	0	(4)
$2OH* \rightarrow H_2O + O* + *$	2	2	2	0	0	(5)
$CH_3^{\bullet} + O* \rightarrow CH_3O*$	0	0	0	0	4	(6)
$2CH_3O* + 5O* \rightarrow 2CO_2 + 3H_2O + 7*$	0	0	0	0	2	(7)
$CO + O* \rightarrow CO_2 + *$	0	0	0	2	0	(8)
$CO_2 + * \rightleftharpoons CO_2*$	0	0	0	0	0	(9)
$4HO_2^{\bullet} \xrightarrow{\text{surf}} 3O_2 + 2H_2O$	0	0	0	0	0	(10)
+						
$4CH_4 + O_2 \rightarrow 4CH_3^{\bullet} + 2H_2O$	(a)					
$4C_2H_6 + O_2 \rightarrow 4C_2H_5^{\bullet} + 2H_2O$	(b)					
$4C_2H_4 + O_2 \rightarrow 4C_2H_3^{\bullet} + 2H_2O$	(c)					
$2CO + O_2 \rightarrow 2CO_2$	(d)					
$4CH_3^{\bullet} + 7O_2 \rightarrow 4CO_2 + 6H_2O$	(e)					

With these t-values the $1 - a$ confidence interval can be determined according to:

$$b_i - t\left(n-p,1-\frac{1}{2}\alpha\right)s(b_i) \le \beta_i \le b_i + t\left(n-p,1-\frac{1}{2}\alpha\right)s(b_i) \qquad (2)$$

The significance of the global regression was expressed by means of the ratio of the mean regression sum of squares to the residual sum of squares, which is distributed according to F (Draper and Smith, 1966).

Kinetic Model Development

The Sn/Li/MgO catalyst is used for model development because more experimental data are available and because the contribution of the gas-phase reactions is lower for this catalyst, as will be shown later. This allows an easier estimation of the kinetic parameters of the catalytic reactions.

Catalytic Reaction Network. The elementary steps on the catalyst surface considered in the kinetic model for Sn/Li/MgO are shown in Table 2. Five global reactions paths (a−e), built up from elementary steps (1−10) and represented by the five columns with stoichiometric numbers, σ, can be distinguished in this model. This way of presenting a complex reaction network was developed by Temkin (1971) and allows a straightforward calculation of the net production rates of the components involved in the catalytic reactions. The set of catalytic reactions, shown in Table 2, is coupled to the gas-phase branched-chain reaction network reported by Chen et al. (1994b). The complete kinetic model thus contains 10 catalytic and 39 gas-phase reactions in which 13 molecules, 10 radicals, and 5 surface components are involved.

Reactions 1, 2, and 5 in Table 2 are very similar to the model proposed by Ito et al. (1985) shown in eq 3 and lead to the same global reaction path (a) for the catalytic generation of methyl radicals.

$$\begin{array}{lll} & & \sigma_i \\ & O_2 + 2Li^+[\,] + 2Li^+O^{2-} \rightleftarrows 4Li^+O^- & 1 \\ & Li^+O^- + CH_4 \rightarrow Li^+OH^- + CH_3^{\bullet} & 4 \\ + & \underline{2Li^+OH^- \rightarrow Li^+O^{2-} + Li^+[\,] + H_2O} & 2 \\ & 4CH_4 + O_2 \rightarrow 4CH_3^{\bullet} + 2H_2O & \end{array} \qquad (3)$$

The first step in this cycle consists of the activation of oxygen through dissociative adsorption. In the second step hydrogen is abstracted from methane by the adsorbed oxygen species, and in the third step the active sites are regenerated via the desorption of water. Several other mechanisms were proposed for the adsorption of oxygen on the catalyst surface. McCarty (1992) used a two-step mechanism in which the adsorption of dioxygen on a vacant site is followed by its rate-determining dissociation to form two hydrogen-abstracting species. Aparicio et al. (1991) also used a two-step oxygen adsorption to describe the kinetics over Li/MgO.

Steady-state transient isotopic kinetic experiments performed by Nibbelke et al. (1995) showed that oxygen was dissociatively adsorbed on both Li/MgO and Sn/Li/MgO. Oxygen-isotope exchange experiments over lined-out Sn/Li/MgO (Nibbelke et al., 1995) could be simulated assuming single-step dissociative adsorption of oxygen. This, plus the modeling results described later, supported the hypothesis to use dissociatively adsorbed oxygen, O*, formed in a one-step adsorption step as the hydrogen-abstracting species in this work.

In reaction 2 of Table 2, hydrogen is abstracted from methane by the adsorbed oxygen, leading to methyl radicals. The question of whether methane is adsorbed on the catalyst surface prior to hydrogen abstraction or whether hydrogen abstraction takes place through an Eley−Rideal step has been an important discussion topic in the literature. Both TAP experiments (Buyevskaya et al., 1994; Mallens et al., 1996) and SSTIKA experiments (Nibbelke et al., 1995) showed that ethane, the product of the coupling of two methyl radicals, leaves the reactor at the same time as the inert tracer, indicating that no surface intermediates are involved in the production of ethane. This can only be explained when methyl radicals are produced through an Eley−Rideal step.

If the catalyst is capable of abstracting a hydrogen radical from methane, it is likely that it can also abstract a hydrogen radical from ethane, reaction 3, because the C−H bond strength in ethane is 20 kJ mol^{-1} lower than that in methane (Lide, 1991). Hydrogen abstraction from ethene, reaction 4, is also considered possible even though the C−H bond in ethene is 5 kJ mol^{-1} stronger than that in methane. The hydrogen abstraction from ethane can be considered as a desired reaction since it leads to an ethyl radical, which mainly reacts further to ethene through the branched chain reactions in the gas phase; see Chen et al. (1994a). Hydrogen abstraction from ethene is an undesired reaction because it leads to the vinyl radical, which is an important source of carbon monoxide in the gas-phase reactions (Chen et al., 1994a).

Regeneration of active sites was assumed to occur through the desorption of water, reaction 5. This is in line with the regeneration reactions used by McCarty (1992) and Aparicio et al. (1991). Krylov (1993) proposed the following step for the regeneration of active sites:

$$4OH* + O_2 \rightarrow 4O* + 2H_2O \qquad (4)$$

This reaction is not elementary but proceeds through intermediate steps in which possibly $OH^{\bullet}$ or $HO_2^{\bullet}$ radicals are involved. Note that eq 4 is the sum of 2 times reaction 5 and reaction 1 in Table 2.

Chen et al. (1994b) discussed experiments in which ethane was added to the feed stream and showed that regeneration of active sites through water desorption

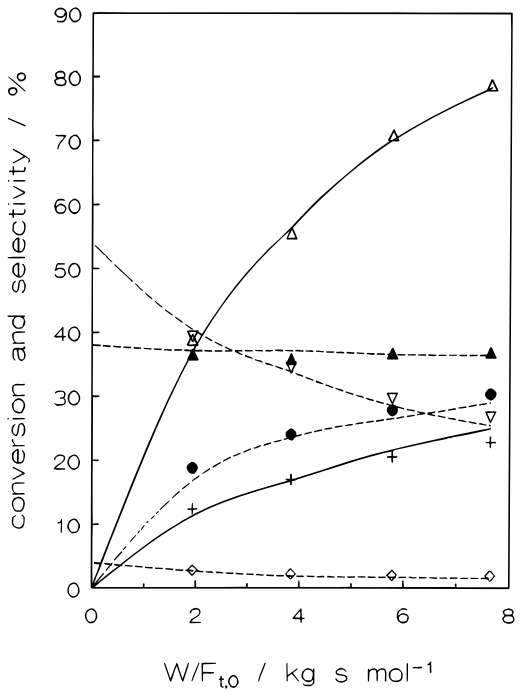

Figure 2. Conversions (—) and selectivities (- - -) vs space time. Lines: calculated using the heterogeneous reactor model equations of Couwenberg et al. (1996) and the heterogeneous reactions of Table 2 with corresponding kinetic parameters of Table 3 coupled to the gas-phase reaction network of Chen et al. (1994b). Points: experiments. +, CH_4; △, O_2; ▽, C_2H_6; ●, C_2H_4; ◇, CO; ▲, CO_2. Conditions: p = 125 kPa, T = 1023 K, $CH_4/O_2|_0$ = 3.6. Catalyst: Sn/Li/MgO.

is not a potentially instantaneous reaction. TAP experiments (Mallens, 1996) showed that the catalyst contains a pool of hydrogen atoms probably in the form of hydroxy groups. After being under reaction conditions for some time, CD_4 was pulsed over the catalyst bed, and some exchange products, e.g., CD_3H, were detected. Therefore, the regeneration, reaction 5, was assumed to be a kinetically significant step, in contrast to what is reported by Shi et al. (1992), Tung and Lobban (1992), and Coulter and Goodman (1993).

An experiment in which the space time was varied in the presence of Sn/Li/MgO (see Figure 2) showed that the initial selectivity toward carbon dioxide is not zero. This implies that carbon dioxide is a primary product, i.e., not produced via a stable intermediate. Therefore, a direct catalytic route toward carbon dioxide must exist since in the gas-phase reaction network it originates from the oxidation of carbon monoxide. Several routes for direct CO_x formation on the catalyst surface were proposed in the literature. McCarty (1992) used the following set of elementary catalytic reactions with a methoxy species as the intermediate:

$$\begin{aligned} CH_3^{\bullet} + O* &\rightleftarrows CH_3O* \\ CH_3O* + O* &\rightleftarrows CH_2O + OH* + * \end{aligned} \qquad (5)$$

The formaldehyde subsequently leads to carbon monoxide through the gas-phase chain reactions. This sequence of catalytic reactions cannot account for the primary carbon dioxide formation, since carbon monoxide is a stable intermediate. If the rate coefficient of catalytic carbon monoxide oxidation, reaction 8 in Table 2, would be sufficiently high to allow one to consider carbon monoxide as a reactive intermediate, this latter constraint can be overcome. However, the experiments

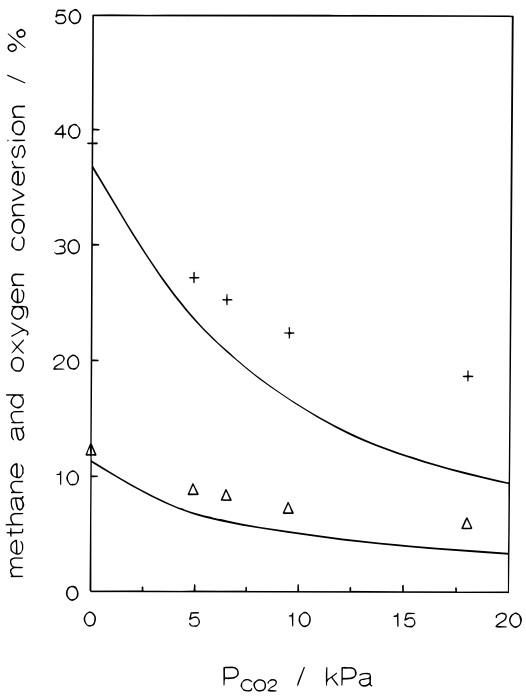

Figure 3. Methane (+) and oxygen (△) conversion vs inlet partial pressure of CO_2. Lines: calculated using the heterogeneous reactor model equations of Couwenberg et al. (1996) and the heterogeneous reactions of Table 2 with corresponding kinetic parameters of Table 3 coupled to the gas-phase reaction network of Chen et al. (1994b). Points: experiments. Conditions: p = 135 kPa, T = 1023 K, $CH_4/O_2|_0$ = 4.0. Catalyst: Sn/Li/MgO.

show a maximum initial selectivity toward carbon monoxide of approximately 15%. Such a high value could never be reached when carbon monoxide is a reactive intermediate. Aparicio et al. (1991) mentioned the reversible adsorption of a methyl radical on O*, leading to a methoxy species. This methoxy species subsequently leads to carbon dioxide through a series of steps which are potentially infinitely fast. Such a series of reactions on the catalyst surface could explain the primary formation of carbon dioxide. Tong and Lunsford (1991) showed that methyl radicals can be oxidized on the catalyst surface by feeding methyl radicals to a bed with a Li/MgO catalyst. Furthermore, modeling of SSTIKA experiments over this catalyst (Nibbelke et al., 1995) revealed that a surface species with a C-to-O ratio of 1 must be involved in the direct catalytic formation of carbon dioxide. Therefore, reactions 6 and 7 in Table 2 were used to account for the direct catalytic carbon dioxide formation. Obviously reaction 7 is not an elementary step but consists of a series of steps on the catalyst surface, eventually leading to carbon dioxide.

Van der Wiele et al. (1992) clearly showed that carbon monoxide was relatively rapidly converted to carbon dioxide over a Li/MgO catalyst by comparing experiments in the absence and in the presence of a catalyst and by CO oxidation experiments. Similar conclusions were drawn by Peil et al. (1989) and Martin et al. (1989). Also our own experiments at elevated pressure over Li/MgO showed that at high pressure the main difference between experiments in the presence and in the absence of catalyst is the decreasing CO_2-to-CO ratio. Therefore, reaction 8 was included in the catalytic network.

The experiments in which carbon dioxide was added to the feed, presented in Figure 3, clearly show that an increasing concentration of CO_2 decreases the consumption rates of methane and oxygen. Also SSTIKA experiments (Nibbelke et al., 1995), using carbon-labeled carbon dioxide, indicated that carbon dioxide shows a strong interaction with a Li/MgO catalyst. This is probably caused by the formation of carbonates on the catalysts surface which reduces the number of active sites available for reaction. Adsorption of CO_2 at high temperatures is not observed on MgO (Meixner et al., 1992). To be able to describe the experiments at high conversion levels, i.e., when a lot of carbon dioxide is present in the gas stream, the inhibiting effect of CO_2 must be included. This is performed by including reaction 9, where CO_2* stands for a carbonate.

Tulenin et al. (1992) showed that magnesium oxide not only produces radicals but also is a very effective radical quencher. Sanches-Marcano et al. (1992) suggested that a Li/MgO catalyst inhibits the gas-phase oxidation of ethene by quenching the very reactive chain carriers. Chainey et al. (1959) proposed reaction 10 of Table 2 as the most likely heterogeneous termination on metal oxide surfaces. Note that this is not an elementary step. The hydrogen−peroxy radical is one of the most important chain carriers in the gas-phase reaction network (Chen et al., 1991). This reaction, therefore, plays a crucial role in the interplay between the catalytic reactions and the branched-chain reactions in the gas phase, a topic that will be addressed later.

Reactions 2−4 are heterogeneous initiation reactions. The produced radicals react further through the branched-chain reactions in the gas phase, and termination occurs through coupling of methyl radicals in the gas phase as well as on the catalyst surface through reactions 6 and 10. Note that the only consecutive reactions of the C_2 products involving the catalyst consist of hydrogen abstractions. The resulting radicals are further oxidized through the homogeneous gas-phase reactions.

Catalytic Rate Equations. To calculate the reaction rates, the law of mass action was applied to each of the elementary steps in Table 2. Reaction 1 of Table 2 was assumed to be in quasi-equilibrium, because modeling of labeled-oxygen exchange experiments (Nibbelke et al., 1995) revealed that the rates of oxygen ad- and desorption are almost equal and much higher than the rate of hydrogen abstraction. Quasi-equilibrium could also be applied for reaction 9 as the experimental reactor was operated in the steady state; i.e., no catalyst deactivation was observed during an experimental run. All other catalytic steps were assumed to be irreversible. Reaction 7 was assumed to be potentially instantaneous. The rate of the carbon dioxide formation through methyl-radical oxidation on the catalyst surface is therefore determined by the rate of reaction 6. The rate of reaction 10 was assumed to be proportional to the concentration of the hydrogen−peroxy radicals and the specific surface area of the catalyst.

Since reaction 1 is in quasi-equilibrium, the following relation between the fraction of dissociatively-adsorbed oxygen, θ_{O*}, and the fraction of free active sites, θ_*, can be derived, provided the Langmuir assumptions hold:

$$\theta_{O_*} = \sqrt{K_1 C_{O_2}}\theta_* \tag{6}$$

where K_1 is the equilibrium coefficient of reaction 1, m_g^3 mol^{-1}, and C_{O_2} the oxygen concentration, mol m_g^{-3}.

Assuming quasi-equilibrium for reaction 9 leads to:

$$\theta_{CO_2*} = K_9 C_{CO_2}\theta_* \tag{7}$$

Applying the steady-state approximation to the hydroxy species yields for θ_{OH*}:

$$\theta_{OH*} = \left[\left(\frac{k_2 C_{CH_4} + k_3 C_{C_2H_6} + k_4 C_{C_2H_6}}{2k_5}\right)\sqrt{K_1 C_{O_2}}\,\theta_*\right]^{1/2} \quad (8)$$

Since reaction 7 is potentially instantaneous, the fraction of methoxy species on the catalyst, θ_{CH_3O*}, is zero. Together with the condition that the sum of the surface fractions equals 1, eqs 4−6 lead to the following relation for θ_{OH*}:

$$\sqrt{\theta_*} = -\left[\left(\frac{k_2 C_{CH_4} + k_3 C_{C_2H_6} + k_4 C_{C_2H_6}}{2k_5}\right)\sqrt{K_1 C_{O_2}}\right]^{1/2} / [2(1 + \sqrt{K_1 C_{O_2}} + K_9 C_{CO_2})] + \left[\left(\frac{k_2 C_{CH_4} + k_3 C_{C_2H_6} + k_4 C_{C_2H_4}}{2k_5}\right)\sqrt{K_1 C_{O_2}} + 4(1 + \sqrt{K_1 C_{O_2}} + K_9 C_{CO_2})\right]^{1/2} / [2(1 + \sqrt{K_1 C_{O_2}} + K_9 C_{CO_2})] \quad (9)$$

Once θ_* is known, all other surface fractions can be calculated from eqs 6−8. From the surface fractions the catalytic production rates of all components can be calculated, and these are then entered in the reactor model equations accounting for the irreducible mass-transport limitations as proposed by Couwenberg et al. (1996).

Catalytic Kinetic Parameter Determination. The rate and equilibrium coefficients of the catalytic reactions were calculated using Arrhenius and van't Hoff type relations. Since the model consists of eight irreversible and two quasi-equilibrated catalytic reactions, 20 parameters would have to be estimated. This number could be reduced to 12 by the use of physicochemical relations (Boudart and Djéga-Mariadassou, 1984; Dumesic et al., 1993). Moreover, assuming that reaction 7 is potentially instantaneous reduces the number of parameters to 10.

The collision theory can be used to calculate the maximum value of the preexponential factor of the Eley−Rideal steps. Aparicio et al. (1991) directly used these collision frequencies as preexponential factors for the Eley−Rideal steps in their kinetic model, whereas McCarty (1992) used one-tenth of the collision frequency to allow for unfavorable configurational constraints. Sinev (1992) used the collision frequency corrected with a steric factor which could be determined from the analogy between the homogeneous gas-phase reactions and the reactions on the catalyst surface. In this work the preexponential factors of steps 2−4 and 8 were assumed to be equal to the collision frequency. This results in a value of 1.85×10^9 m_g^3 m_p^{-3} s^{-1} for A_2, 1.35×10^9 for A_3, 1.40×10^9 for A_4, and 1.91×10^9 m_g^3 m_p^3 s^{-1} for A_8.

Because reactions 6 and 10 are terminations, the activation energies were assumed to be zero. The activation energies of reactions 2−4 can be coupled through the Polanyi−Semenov relation (Boudart and Djéga-Mariadassou, 1984):

$$|\Delta E_a| = \alpha \Delta |\Delta H_r^0| \quad (10)$$

where α is the Polanyi−Semenov parameter; ΔE_a the difference between the activation energies of two homologous steps, J mol^{-1}; and $\Delta|\Delta H_r|$ the corresponding difference between the reaction enthalpies, J mol^{-1}. Following Semenov, Krylov (1993) assumed that $\alpha = 0.75$ for hydrogen-abstraction reactions on Li/MgO-based catalysts. Because the difference in reaction enthalpy of reactions 2−4 is determined by the difference in the C−H bond strengths, it follows that $E_{a,2} = E_{a,1} - 15$ kJ mol^{-1} and that $E_{a,3} = E_{a,1} + 3.75$ kJ mol^{-1}.

The estimated parameter values with their corresponding *t*-values as well as the fixed and related parameters are shown in Table 3. The *F*-value of the regression amounted to 91 000. The largest value of the binary correlation coefficient between two parameter estimates occurred for the preexponential factors of reactions 5 and 9 and amounted to 0.96. Figure 4 shows the experimental versus the calculated methane and oxygen conversions for all experiments at pressures

Table 3. Kinetic Parameter Estimates with the Corresponding *t*-Values for the Estimates from a Regression of 24 Experiments[a]

reaction	A^b	*t*-value	E_a c.q. ΔH/kJ mol^{-1}	*t*-value
1	2.6×10^{-3}	2.7	−11.8	15
2	1.9×10^9		123.1	160
3	1.4×10^9		108.1	
4	1.4×10^9		127.8	
5	6.9×10^9	6.0	152.7	229
6	3.6×10^6	16.0	0.0	
7	∞		0.0	
8	1.9×10^9		93.7	67
9	5.0×10^{-5}	5.5	−108.4	170
10	1.0×10^{-2}	7.6	0.0	

[a] The heterogeneous reactor model equations from Couwenberg et al. (1995) were applied during the simulations. The catalytic reaction network in Table 3 was coupled to the gas-phase reaction network from Chen et al. (1994b). [b] Units: m_g^3 mol^{-1} (1,9), m_g^3 m_p^{-3} s^{-1} (2,3,4,6,8), mol m_p^{-3} s^{-1} (5), m_g^3 m_c^{-2} s^{-1} (10).

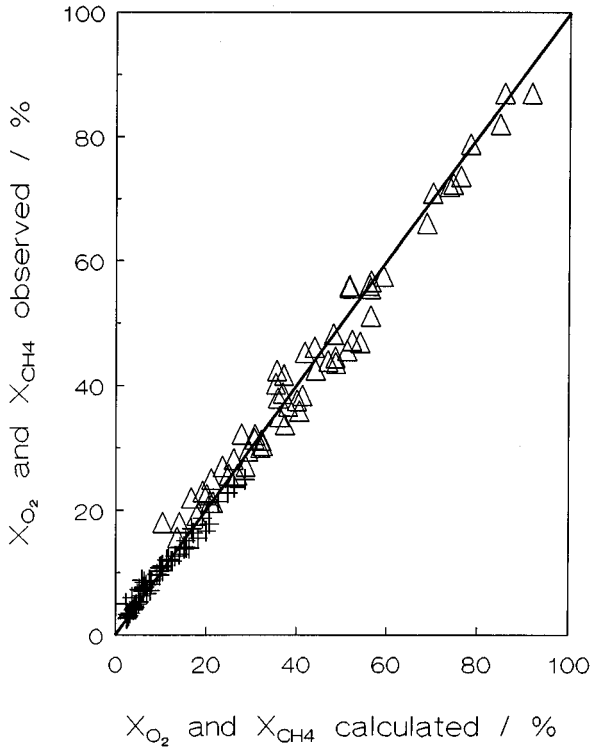

Figure 4. Experimental vs calculated methane (+) and oxygen (△) conversion. Calculated using the heterogeneous reactor model equations of Couwenberg et al. (1996) and the heterogeneous reactions of Table 2 with corresponding kinetic parameters of Table 3 coupled to the gas-phase reaction network of Chen et al. (1994b). Experimental conditions: see Table 1. Catalyst: Sn/Li/MgO.

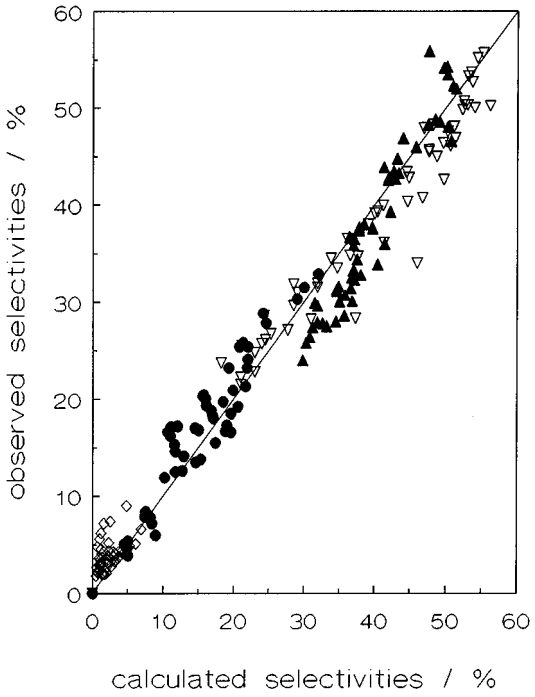

Figure 5. Experimental vs calculated selectivities. ▽, C_2H_6; ●, C_2H_4; ◇, CO; ▲, CO_2. Calculated using the heterogeneous reactor model equations of Couwenberg et al. (1996) and the heterogeneous reactions of Table 2 with corresponding kinetic parameters of Table 3 coupled to the gas-phase reaction network of Chen et al. (1994b). Experimental conditions: see Table 1. Catalyst: Sn/Li/MgO.

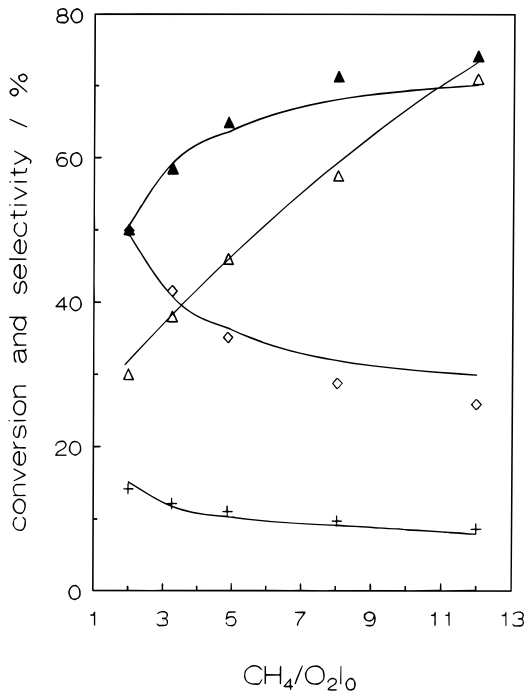

Figure 6. Conversions and selectivities vs the inlet methane-to-oxygen ratio. Lines: calculated using the heterogeneous reactor model equations of Couwenberg et al. (1996) and the heterogeneous reactions of Table 2 with corresponding kinetic parameters of Table 3 coupled to the gas-phase reaction network of Chen et al. (1994b). Points: experiments. +, CH_4; △, O_2; ◇, CO_x; ▲, C_{2+}. Conditions: p = 130 kPa, T = 1023 K, $W/F_{t,0}$ = 2.0 kg s mol^{-1}. Catalyst: Sn/Li/MgO.

lower than 150 kPa. These parity diagrams thus also include experiments which were not used during the parameter estimation. The deviation between the observed and calculated conversions is usually within 15%. Note that the model also adequately predicts the conversion outside the range of conversions used during the parameter estimation, see Table 1. Figure 5 shows the simulated versus the experimental selectivities toward ethane, ethene, carbon monoxide, and carbon dioxide. Clearly, a good agreement between the experimental and calculated selectivities is realized with this kinetic model as well.

Simulation Results

A one-step dissociative oxygen adsorption in quasi-equilibrium is sufficient for an adequate description of the experimental data, as was the case for modeling of the oxygen exchange experiments by Nibbelke et al. (1995) over the same catalyst. This follows most clearly from the experiments in Figure 6 showing the conversions of methane and oxygen and the selectivities toward C_{2+} and CO_x versus the inlet methane-to-oxygen molar ratio. In this experiment the oxygen concentration at the reactor inlet varies from 5 to 1 mol m^{-3}. Clearly, both the conversions and selectivities are adequately simulated using a one-step dissociative oxygen adsorption mechanism. The use of a two-step mechanism in which one of the adsorbed oxygen species is responsible for the oxidation and the other one for the production of methyl radicals did not improve these simulation results. The number of parameters to be estimated would increase by two. Therefore, the one-step oxygen adsorption mechanism was preferred.

The adequate simulation of the selectivities toward carbon dioxide in an experiment in which the space time was varied (see Figure 2) shows that reactions 6 and 7 in Table 2 provide a good route to account for the primary carbon dioxide production.

Carbon monoxide is completely produced through the branched-chain reactions and undergoes consecutive oxidation toward carbon dioxide on the catalyst surface and through the gas-phase chain reactions. Therefore, the good simulation of the slightly decreasing selectivity toward carbon monoxide with increasing space time (see Figure 2) shows that this model correctly accounts for the relative contribution of the gas-phase reactions and consecutive catalytic oxidation of carbon monoxide. The adequate simulation of the ethane and ethene selectivity implies that the contribution of the consecutive oxidation of ethane and ethene is correctly accounted for by reactions 3 and 4 and the corresponding kinetic parameter values.

Clearly, the simulated inhibiting effect of CO_2 addition (see Figure 3) is somewhat more pronounced than the observed effect. Smith and Galuszka (1994) and Al-Zahrani et al. (1994) modeled the effect of CO_2 addition using Hougen−Watson rate equations. In both papers the inhibiting effect of CO_2 addition was accounted for by a reaction similar to reaction 9. Smith and Galuszka (1994) found deviations between experimental and simulated conversions comparable to the deviations reported in this work. The deviations reported by Al-Zahrani et al. (1994) were much smaller, but the maximum CO_2 partial pressure in their experiments was limited to 0.5 kPa. The reason for the observed deviations can be that the formation of a carbonate phase cannot completely be described by a simple reaction like reaction 9 but requires a mechanism involving complex solid-state reactions. Furthermore, the formation of carbonates could also influence the kinetics of active-site regeneration and/or oxygen acti-

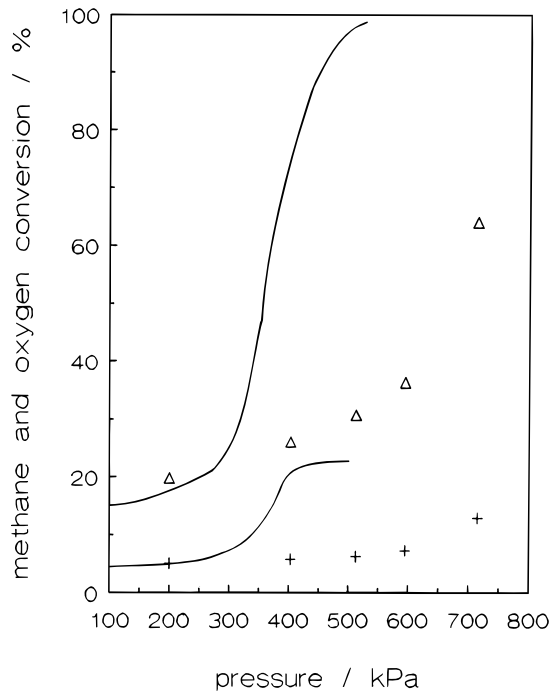

Figure 7. Methane (+) and oxygen (△) conversion vs pressure. Lines: calculated using the heterogeneous reactor model equations of Couwenberg et al. (1996) and the heterogeneous reactions of Table 2 with corresponding kinetic parameters of Table 3 coupled to the gas-phase reaction network of Chen et al. (1994b). Points: experiments. Conditions: $T = 985$ K, $CH_4/O_2|_0 = 4.0$, $W/F_{t,0} = 1$ kg s mol^{-1}. Catalyst: Sn/Li/MgO.

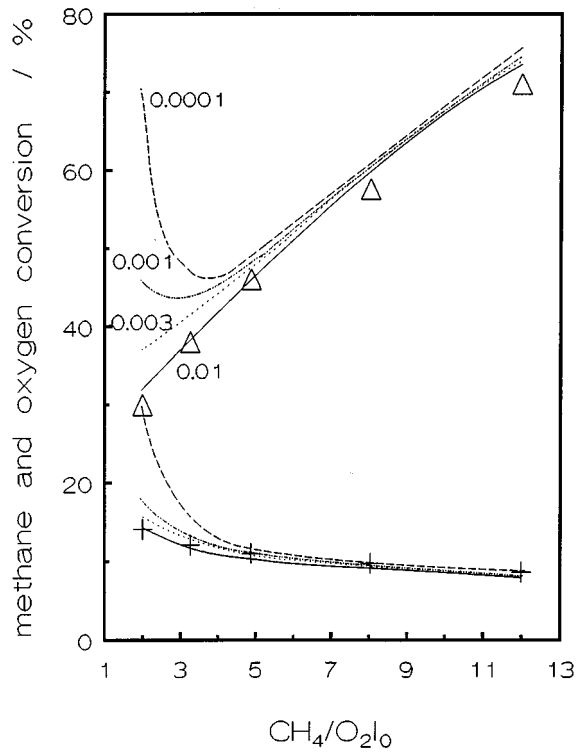

Figure 8. Methane (+) and oxygen (△) conversion vs the inlet methane-to-oxygen ratio. Full lines: calculated using the heterogeneous reactor model equations of Couwenberg et al. (1996) and the heterogeneous reactions of Table 2 with corresponding kinetic parameters of Table 3 coupled to the gas-phase reaction network of Chen et al. (1994b). Dashed lines: calculated with the same model but with values of k_{10} as indicated in the figure. Points: experimental. Conditions: see Figure 6.

vation steps. During the experiments without cofeeding carbon dioxide these effects are not significant due to the relatively low concentrations of carbon dioxide. This can be seen in Figure 2 where the simulations at high methane conversion are still very adequate.

Figure 7 shows calculated and experimental conversions of methane and oxygen versus the total pressure. The experimental conversions of methane and oxygen are hardly influenced by the pressure up to 600 kPa; i.e., the global reaction order is approximately zero. It can be shown that such a behavior requires that regeneration of active sites through water desorption is a kinetically significant step, i.e., not potentially instantaneous, in line with the conclusions of Chen et al. (1994b).

The trends in the conversions are only adequately described up to a total pressure of 300 kPa. Above this pressure the calculated conversions increase strongly. This corresponds to the ignition of the branched chain reactions in the gas phase. The latter is also observed in the absence of catalyst from 300 kPa on (Chen et al., 1994a). In the presence of catalyst this ignition behavior is observed as well, however, from pressures of 600 kPa on only.

The simulations show that the effect of the total pressure on the rate of the catalytic reactions is adequately described by eqs 6−9 and the corresponding parameter estimates in Table 3, because these equations simulate the zero-order behavior with respect to the total pressure at pressures where the methane and oxygen conversion are mainly determined by the catalytic reactions. The gas-phase reaction network reported by Chen et al. (1994a) describes the effect of pressure in the absence of catalyst adequately as well. The simulated ignition of the branched-chain reactions during the catalyzed process at a too low pressure must thus be caused by an overestimation of the relative importance of the gas-phase chain reactions at elevated pressures.

An important reaction determining the relative importance of the branched-chain reactions is the heterogeneous termination reaction 10 in Table 2. This is shown in Figure 8 in which the conversions of methane and oxygen at 130 kPa are plotted versus the inlet methane-to-oxygen ratio for Sn/Li/MgO. The full lines correspond to the calculations using the kinetic parameter estimates listed in Table 3. The dashed lines correspond to calculations with the same kinetic model but lower values for the rate coefficient of the heterogeneous termination reaction 10. Obviously, the conversions of methane and oxygen are simulated adequately in all cases at high inlet methane-to-oxygen ratios. At low inlet methane-to-oxygen ratios the importance of the branched-chain reactions increases when the rate coefficient of the heterogeneous termination is lowered. The simulated oxygen conversions are rather sensitive to relatively small changes in the rate coefficient of the heterogeneous termination. Decreasing the rate coefficient by a factor of 3 results in an increase in the oxygen conversion from 31 to 37% at a methane-to-oxygen ratio of 2, while decreasing k_{10} by a factor of 100 results in a calculated oxygen conversion of 70%. Furthermore, lowering the rate coefficient of the heterogeneous termination reaction results in lower calculated selectivities toward C_2 products, due to the increasing importance of the gas-phase chain reactions.

During the simulation of the experiment at 400 kPa shown in Figure 7, the calculated rate of initiation plus branching through the gas-phase chain reactions equals 24 mol m_r^{-3} s^{-1}, whereas the rate of initiation through

Table 4. Interstitial and Intraparticle Rates in mol m_r^{-3} s^{-1} for Sn/Li/MgO and Li/MgO[a]

	Sn/Li/MgO		Li/MgO	
	intraparticle	interstitial	intraparticle	interstitial
initiation				
catalytic	7.8		0.19	
gas phase	2.1×10^{-2}	0.13	6.9×10^{-3}	0.12
termination				
catalytic	3.7		0.1	
gas phase	4.1	1.5	8.5×10^{-2}	0.18
CH_4 consumption				
catalytic	7.4		0.17	
gas phase	0.36	0.78	3.9×10^{-2}	0.32
O_2 consumption				
catalytic	8.2		0.19	
gas phase	0.30	0.38	2.9×10^{-2}	0.14
CH_3 consumption				
cat. oxidation	3.5		7.8×10^{-2}	
coupling	4.0	1.54	9.0×10^{-2}	0.19
oxidation	0.05	0.29	1.2×10^{-2}	0.08
hydrogen abstraction	0.16	0.35	1.8×10^{-2}	0.14

[a] Conditions: $T = 1023$ K, $p = 110$ kPa, $CH_4/O_2|_0 = 4.0$, $X_{O_2} = 19\%$, $d_p = 0.25$ mm.

the catalytic reactions only equals 1.5 mol m_r^{-3} s^{-1}. In the previous paragraph, it was shown that the contribution of the gas-phase reactions is sensitive toward the value of the rate coefficient for the heterogeneous termination reaction 10. Therefore, the rate coefficient of the heterogeneous termination reaction 10 was tentatively increased to the collision frequency, corresponding to an increase by a factor of 10^4. This shifted up the pressure where the branched-chain reactions overtake the catalytic reactions to a total pressure of 450 kPa. However, the resulting agreement with the experiments at low pressure is much worse. Especially, the selectivity toward carbon monoxide would be simulated too low as a result of the decrease of the relative importance of the gas-phase reactions at low pressure. Therefore, a more likely reason for the observed deviations is that the mass-transfer rate from the interstitial phase to the intraparticle phase is underestimated at high pressure. Higher rates of mass transfer lead to a higher contribution of the heterogeneous termination on the termination of the branched-chain reactions in the interstitial phase. In the reactor model used for the simulations of the experiments, mass transfer is described by molecular diffusion only (Couwenberg et al., 1996). With increasing pressure, the diffusion coefficient decreases, resulting in a lower rate of mass transfer. Furthermore, at high pressure, the turbulent contribution to mass transfer may no longer be negligible.

Relative Importance of Gas-Phase Reactions at Atmospheric Pressure

The simulations in Figures 2, 6, and 7 show that the model accounts correctly for the relative importance of the gas-phase reactions at low pressures. Therefore, a contribution analysis will be performed using an experiment at 110 kPa. This analysis will focus on where the main initiation and termination reactions take place and where and through which reactions consumption and production of the main components occur.

Sn/Li/MgO. Initiation and Termination. Table 4 shows the calculated rates of initiation and termination through the gas-phase reactions and the catalytic reactions both in the center of the interstitial phase and in the center of the intraparticle phase per unit reactor volume. The latter normalization was performed by taking into account the bed and pellet porosity as well as the bed dilution.

The table shows that 98% of the initiation occurs through the catalytic reactions, of which 95% is accounted for by reaction 2 in Table 3, i.e., the catalytic methyl-radical production. The gas-phase initiation, in which chain branching reactions were included, occurs for 60% through branching reaction (G1):

$$H_2O_2 + M \rightarrow 2OH^\bullet + M \qquad \text{(G1)}$$

In the absence of catalyst, this branching reaction is the most important source of radicals (Chen et al., 1994a). Termination occurs for approximately 60% through gas-phase reactions and for 40% through catalytic reactions. The hydrogen−peroxy radical quenching through reaction 10 in Table 2 accounts for 8%, and the methyl-radical oxidation reaction 6 accounts for 92% of the catalytic termination. Termination through the gas-phase reactions, in analogy with the process in the absence of catalyst, consists for over 99% of coupling of two methyl radicals. Note that the sums of the rates of initiation and termination in the center of the intraparticle phase are equal and thus that the concentration of all radicals in the center of the pellet is completely determined by the balance between production and consumption, as was already concluded by Couwenberg et al. (1996). The rates of initiation and termination in the center of the interstitial phase are not equal due to a significant contribution of catalytically produced methyl radicals which are released into the interstitial phase.

Methane and Oxygen Consumption. Methane consumption occurs through catalytic reaction 2 in Table 2 and through several gas-phase reactions (Chen et al., 1994b), of which reactions G2 and G3 are the most important ones:

$$CH_4 + H^\bullet \rightarrow CH_3^\bullet + H_2 \qquad \text{(G2)}$$

$$CH_4 + OH^\bullet \rightarrow CH_3^\bullet + H_2O \qquad \text{(G3)}$$

In all these reactions, methane is converted into methyl radicals. At the conditions given in Table 4, 87% of the methane is converted through the catalytic reaction 2. Thirteen percent is converted through the gas-phase reactions of which 4% takes place in the intraparticle phase and 9% in the interstitial phase. Oxygen consumption was found to occur for 92% through the

catalytic reactions, for 4% through the branched-chain reactions in the intraparticle phase, and for 4% in the interstitial phase. Sixty-seven percent of the oxygen is consumed through global catalytic reaction path (e) in Table 2, i.e., the direct catalytic formation of carbon dioxide. Shi et al. (1992) performed a similar analysis and found that maximally 15% of the methane consumption was accounted for by reactions in the gas phase.

Methyl-Radical Consumption. The methyl radicals produced from methane are consumed through coupling reaction G4 in the gas phase:

$$CH_3^\bullet + CH_3^\bullet + M \rightarrow C_2H_6 + M \qquad \text{(G4)}$$

through several gas-phase oxidation reactions (Chen et al., 1994b) of which reaction G5 is the most important one:

$$CH_3^\bullet + HO_2^\bullet \rightarrow CH_3O^\bullet + OH^\bullet \qquad \text{(G5)}$$

through gas-phase hydrogen-abstraction reactions in which the methyl radical is converted back into methane, and through catalytic oxidation reaction 6 in Table 2. The carbon-containing components produced in gas-phase reactions, like $CH_3O^\bullet$ in (G5), are precursors for carbon monoxide formation. The methyl-radical consumption reactions determine the primary selectivity toward carbon monoxide, carbon dioxide, and ethane. Table 4 shows the rates of all four types of methyl-radical consumption reactions both in the interstitial and in the intraparticle phase. Coupling in the pores of the catalyst accounts for 40% and coupling in the interstitial phase accounts for 16% of the methyl-radical consumption. The sum of the interstitial and intraparticle gas-phase oxidation rates accounts for 3% of the total methyl-radical consumption. This contribution increases with increasing space time due to an increase in the concentrations of most radicals. Thirty-six percent of the methyl radicals are consumed through catalytic oxidation, and the remaining 5% are transformed back to methane. Table 4 shows that the coupling selectivity of the methyl radicals, i.e., the ratio of the rate of coupling to the sum of the rates of coupling and oxidation, is higher in the interstitial phase than in the intraparticle phase. This shows that at these conditions the catalytic oxidation of the methyl radicals, rather than the branched-chain reactions in the gas phase, is the selectivity limiting reaction for Sn/Li/MgO.

Li/MgO. The above contribution analysis showed that the relative contribution of the gas-phase reactions is rather low for Sn/Li/MgO at the conditions where the model accurately describes the experimental observations. Experiments on Li/MgO showed that for this catalyst the relative contribution of the gas-phase chain reactions is more important but not yet dominant (Couwenberg, 1995). To obtain more insights, the model for Sn/Li/MgO was adapted in such a way that the experiments over Li/MgO are adequately described. To do so, the preexponential factors for catalytic reactions 1, 5, 6, and 9 were adjusted to 4.6×10^{-5} m_g^3 mol^{-1}, 1.0×10^9 mol m_p^{-3} s^{-1}, 8.3×10^5 m_g^3 m_p^{-3} s^{-1}, and 4.0×10^{-5} m_g^3 mol^{-1}. All other parameters were only corrected for the difference in the specific surface area.

With this model, a contribution analysis is carried out at the same conditions as the contribution analysis for Sn/Li/MgO; see Table 4. To reach the same conversion, a higher space time was applied. The initiation of the chain reactions occurs for 61% through the catalytic initiation reactions, for 2% through gas-phase reaction in the intraparticle phase, and for 37% in the interstitial phase. Termination on the catalyst surface now accounts for 28% of the total termination rate. Twenty-three percent occurs through coupling in the pores of the catalyst, and the remaining 49% is accounted for by coupling in the interstitial phase.

Thirty-two percent of the methane consumption takes place on the catalyst surface, 7% through gas-phase reaction in the pores of the catalyst, and 61% in the interstitial phase. Oxygen consumption occurs for 52% on the catalyst surface, for 8% through gas-phase reactions in the pores of the catalyst, and for 40% in the interstitial phase. Methyl-radical coupling in the intraparticle phase accounts for 15% of the methyl-radical consumption, and coupling in the interstitial phase accounts for 31%. Thirteen percent of the methyl radicals is consumed through catalytic oxidation. Two percent is consumed through gas-phase oxidation reactions in the intraparticle phase, and 13% is consumed through oxidation in the interstitial phase. Twenty-six percent of the methyl radicals is involved in hydrogen abstractions leading to methane.

Finally, it should be noted that even though the relative importance of the gas-phase reactions is much higher for Li/MgO than for Sn/Li/MgO the coupling selectivity toward C_2 products is higher for Li/MgO. This is caused by the higher coupling selectivity in the interstitial phase at the conditions used for the contribution analysis. For Li/MgO the contribution of the reactions in the interstitial phase is much higher than that for Sn/Li/MgO, resulting in a higher selectivity.

Effect of Process Conditions. It was shown previously that at pressures below 300 kPa the conversions of methane and oxygen are for over 85% determined by the catalytic reactions for Sn/Li/MgO. The consumption rate of methyl radicals determines the primary selectivity and occurs for 90% through coupling in the gas phase and oxidation on the catalyst surface. This implies that the trends in the observed effects of the process conditions at low pressure can be explained based on the catalytic reactions and the coupling reaction in the gas phase. The observed effects can be explained on the basis of kinetic considerations, i.e., are not influenced by stoichiometric limitations, except for oxygen conversion.

For Li/MgO an analysis of the effects of process conditions based on only catalytic methyl-radical production and oxidation and coupling in the gas phase is not possible due to the much higher contribution of the gas-phase chain reactions.

Inlet Methane-to-Oxygen Ratio. Increasing the inlet methane-to-oxygen ratio decreased methane conversion and increased oxygen conversion and C_2 selectivity; see Figure 6. From eqs 6−9, with the parameter estimates shown in Table 3, it follows that reducing the oxygen concentration from 5 to 1 mol m^{-3} at 1023 K and 125 kPa results in a decreasing concentration of the absorbed oxygen, O*, from 0.024 to 0.015. The lower concentration of the adsorbed oxygen leads to a lower rate of methyl-radical production. As mentioned previously the methyl-radical concentration in the center of the catalyst pellet is determined by the balance between production and consumption:

$$k_2 C_{CH_4} \theta_{O^*} = k_6 C_{CH_3^*} \theta_{O^*} + 2k_{G4} C_{CH_3^*}{}^2 \epsilon_c \qquad (11)$$

where k_{G4} is the rate coefficient of the coupling reaction

in the gas phase; see Chen et al. (1994b). Solving eq 13 for the $CH_3^{\bullet}$ concentration shows that lowering the oxygen concentration from 5 to 1 mol m_g^{-3} leads to a slight increase in the concentration of the methyl radical from 1.8×10^{-3} to 1.9×10 mol m_g^{-3}. This is due to the lower consumption rate through catalytic oxidation, reaction 6. The selectivity which is mainly determined by:

$$S_{C_2} = \frac{2k_{G4}C_{CH_3^*}{}^2\epsilon_c}{2k_{G4}C_{CH_3^*}{}^2\epsilon_c + k_6C_{CH_3^*}\theta_{O^*}} \qquad (12)$$

thus increases with increasing $CH_4/O_2|_0$ ratio.

Temperature. The observed increase in conversion and selectivity with increasing temperature can be explained in a similar way. At an inlet methane-to-oxygen ratio of 4.0 and at 125 kPa the concentration of adsorbed oxygen increases from 0.016 to 0.020, with the temperature increasing from 973 to 1023 K. Together with the Arrhenius dependency of the rate coefficient of catalytic reaction 2, this leads to a strong increase in the methane and oxygen consumption rates and thus in increasing conversions. The methyl-radical concentration in the center of the pellet increases from 1.1×10^{-3} to 1.9×10^{-3} mol m_g^{-3}, i.e., is more pronounced than the increase in the concentration of the adsorbed oxygen. Therefore, the rate of coupling of methyl radicals will increase more than the rate of catalytic methyl-radical oxidation, and thus the selectivity will increase with increasing temperature, as long as the branched chains do not become dominant.

Because the selectivity increases with increasing temperature, the highest yield toward C_2 products for Sn/Li/MgO can probably be obtained at temperatures higher than the maximum temperature in Table 1, i.e., 1023 K. Therefore, an experiment was performed at a temperature of 1123 K, a pressure of 130 kPa, and an inlet methane-to-oxygen ratio of 2.0. This resulted in a yield of 20%, which is indeed significantly higher than the maximum yield of 14% obtained during the kinetic experiments.

Conclusions

A kinetic model for the heterogeneously catalyzed oxidative coupling of methane, accounting for irreducible mass-transfer limitations of reactive gas-phase intermediates, was developed. This model adequately describes the experimental observations over a broad range of operating conditions. A quantitative analysis of the relative contribution of gas-phase chain reactions and catalytic reactions showed that the effects of process conditions on the selectivity can be described in terms of steady-state concentrations of oxygen ad-atoms and methyl radicals in the case of Sn/Li/MgO: the increase of oxygen ad-atom concentration which follows a temperature increase is more than compensated by an increase in the methyl-radical concentration, leading to a higher selectivity. The increasing selectivity with increasing inlet methane-to-oxygen ratio can be explained similarly. The interaction of Sn/Li/MgO with ethane and ethene is limited to hydrogen abstractions. Heterogeneous termination of the hydrogen−peroxy radicals, produced during the branched-chain reactions in the gas phase, was found to be a crucial reaction to describe the relative importance of the gas-phase reactions.

At atmospheric pressure the major part of the methane and oxygen consumption occurs on the surface of the catalyst. The rate of initiation of the chain reactions is mainly determined by the catalytic production of methyl radicals. Termination occurs through coupling of methyl radicals in the gas phase, through oxidation of methyl radicals on the catalyst surface, and through quenching of hydrogen−peroxy radicals on the catalyst surface. For the Li/MgO catalyst the relative importance of the gas-phase reactions at similar conditions is more important than for Sn/Li/MgO but does not completely determine the rates. On both catalyst branched chains develop with increasing pressure and lead to higher conversions.

Since the irreducible mass-transport limitations are accounted for during the parameter estimation, intrinsic values for the kinetic parameters could be obtained. These kinetic parameters can therefore be applied in a straightforward way for the design of an industrial-scale reactor, either with a fixed or fluidized bed.

Acknowledgment

The financial support provided by the commission of the European Communities in the framework of the JOULE programme, subprogramme Energy from Fossil Sources, Hydrocarbons, No. JOUF-0044-C, is gratefully acknowledged.

Nomenclature

Roman Symbols

A = preexponential factor (Arrhenius), reaction dependent
b = parameter estimates
C_i = concentration of component i, mol m^{-3}
d_p = pellet diameter, m
d_t = reactor diameter, m
E_a = activation energy, J mol^{-1}
F = ratio of mean regression sum of squares to the residual sum of squares
ΔH_r^0 = standard reaction enthalpy, J mol^{-1}
K = equilibrium coefficient, reaction dependent
L = catalyst bed length, m
k = rate coefficient, reaction dependent
p = pressure, Pa
S = selectivity toward component i
s = estimated standard deviation
T = temperature, K
$t(n-p,1-\alpha/2)$ = tabulated $\alpha/2$-percentage point of the t-distribution with $n - p$ degrees of freedom
y_i = mole fraction of component i, mol mol^{-1}
X_i = conversion of component i

Greek Symbols

α = Polanyi−Semenov parameter
β = parameter
ϵ_c = catalyst porosity, $m_g^3 m_c^{-3}$
θ_i = fraction of the surface covered by species i
σ^{hk} = element of the error variance−covariance matrix

Subscripts

c = catalyst
g = gas

Literature Cited

Al-Zahrani, S.; Song, Q.; Lobban, L. L. Effect of CO_2 during Oxidative Coupling of Methane over Li/MgO: Mechanisms and Models. *Ind. Eng. Chem. Res.* **1994**, *33* (2), 251.

Aparicio, L. M.; Rossini, S. A.; Sanfilippo, D. G.; Rekoske, J. E.; Treviño, A. A.; Dumesic, J. A. Microkinetic Analysis of Methane Dimerization Reaction. *Ind. Eng. Chem. Res.* **1991**, *30*, 2114.

Bistolfi, M.; Fornasari, G.; Molinari, M.; Palmery, S.; Dente, M.; Ranzi, E. Kinetic Model for Methane Oxidative Coupling Reactors. *Chem. Eng. Sci.* **1992**, *47* (9−11), 2647.

Boudart, M. *Kinetics of Chemical Processes*, 1st ed.; Prentice Hall: Englewood Cliffs, NJ, 1968.

Boudart, M.; Djéga-Mariadassou, G. *Kinetics of Heterogeneous Catalytic Reactions*; Princeton University Press: Princeton, NJ, 1984; p 121.

Buyevskaya, O. V.; Rothaemel, M.; Zanthoff, H.; Baerns, M. Transient Studies on Reaction Steps in the Oxidative Coupling of CH_4 on Catalytic surfaces of MgO and Sm_2O_3. *J. Catal.* **1994**, *146*, 346.

Chainey, D. E.; Davies, D. A.; Davis, A.; Hoare, D. E.; Protheroe, J.; Walsh, A. D. Effects of Surfaces on Combustion of Methane and Mode of Interaction of Antiknocks Containing Metals. *7th Symposium on Combustion*; Butterworth Scientific Publications: London, 1959; p 183.

Chen, Q.; Hoebink, J. H. B. J.; Marin, G. B. Kinetics of the Oxidative Coupling of Methane at Atmospheric Pressure in the Absence of Catalyst. *Ind. Eng. Chem. Res.* **1991**, *30*, 2088.

Chen, Q.; Couwenberg, P. M.; Marin, G. B. Effect of Pressure on the Oxidative Coupling of Methane in the Absence of Catalyst. *AIChE. J.* **1994a**, *40* (3), 521.

Chen, Q.; Couwenberg, P. M.; Marin, G. B. The Oxidative Coupling of Methane with Cofeeding of Ethane. *Catal. Today* **1994b**, *21*, 309.

Coulter, K.; Goodman, D. W. The Role of Carbon Dioxide in the Oxidative Dimerization of Methane over Li/MgO. *Catal. Lett.* **1993**, *20*, 169.

Couwenberg, P. M. Gas Phase Chain Reactions Catalyzed by Solids: The Oxidative Coupling of Methane. Ph.D. Thesis, Eindhoven University of Technology, Eindhoven, The Netherlands, 1995.

Couwenberg, P. M.; Chen, Q.; Marin, G. B. Irreducible Mass-Transport Limitations during a Heterogeneously Catalyzed Gas-Phase Chain Reaction: The Oxidative Coupling of Methane. *Ind. Eng. Chem. Res.* **1996**, *35*, 415.

Draper, N. R.; Smith, H. *Applied Regression Analysis*; Wiley: New York, 1966.

Dumesic, J. A.; Rudd, D. F.; Aparicio, L. M.; Rekoske, J. E.; Treviño, A. A. *The Microkinetics of Heterogeneous Catalysis*; ACS professional reference book; American Chemical Society: Washington, DC, 1993.

Ekström, A.; Regtop, R.; Bhargava, S. Effect of Pressure on the Oxidative Coupling Reaction of Methane. *Appl. Catal.* **1990**, *62*, 253.

Fang, T.; Yeh, C. T. Interactions of Methane with ThO_2/SiO_2 surface at 1073 K. *J. Catal.* **1981**, *69*, 227.

Froment, G. F.; Bischoff, K. B. *Chemical Reactor Analysis and Design*; John Wiley and Sons: London, 1990.

Froment, G. F.; Hosten, L. Catalytic Kinetics: Modelling. In *Catalysis Science and Technology*; Anderson, J. R., Boudart, M., Eds.; Springer Verlag: Berlin, 1981; p 98.

Gleaves, J. T.; Ebner, J. R.; Kuechler, T. C. Temporal Analysis of Products (TAP). A Unique Catalyst Evaluation System with Submillisecond Time Resolution. *Catal. Rev., Sci. Eng.* **1988**, *30* (1), 49.

Hoebink, J. H. B. J.; Couwenberg, P. M.; Marin, G. B Fixed Bed Reactor Design for Gas-Phase Chain Reactions Catalysed by Solids: The Oxidative Coupling of Methane. *Chem. Eng. Sci.* **1994**, *49* (24B), 5453.

Ito, T.; Wang, J.-X.; Lin, C. H.; Lunsford, J. H. Oxidative Dimerization of Methane over a Lithium Promoted Magnesium Oxide Catalyst. *J. Am. Chem. Soc.* **1985**, *107*, 5062.

Korf, S. J.; Roos, J. A.; Veltman, L. J.; van Ommen, J. G.; Ross, J. R. H. Effect of Additives on Lithium Doped Magnesium Oxide Catalysts Used in the Oxidative Coupling of Methane. *Appl. Catal.* **1989**, *56*, 119.

Krylov, O. V. Catalytic Reactions of Partial Methane Oxidation. *Catal. Today* **1993**, *18* (3), 209.

Lide, D. R. *Handbook of Chemistry and Physics*; CRC Press: Boca Raton, FL, 1991.

Lunsford, J. H. The Catalytic Conversion of Methane to Higher Hydrocarbons. *Catal. Today* **1990**, *5*, 235.

Mallens, E. P. J. A Reaction Path Analysis of the Catalytic Partial Oxidation by Transient Experiments. Ph.D. Thesis, Eindhoven University of Technology, 1996.

Mallens, E. P. J.; Hoebink, J. H. B. J.; Marin, G. B. The Oxidative Coupling of Methane over Tin Promoted Lithium Magnesium Oxide: a TAP Investigation. In *Studies in Surface Science and Catalysis*; Curry-Hyde, H. E., Howe, R. F., Eds.; Elsevier Science B.V.: Amsterdam, The Netherlands, 1994; Vol. 81, p 205.

Mallens, E. P. J.; Hoebink, J. H. B. J.; Marin, G. B. An Investigation of the Oxygen Pathways in the Oxidative Coupling of Methane over MgO Based Catalysts. *J. Catal.* **1996**, submitted for publication.

Marquardt, D. W. An Algorithm for Least-Squares Estimation of Nonlinear Parameters. *J. Soc. Ind. Appl. Math.* **1963**, *11* (2), 431.

Martin, G. A.; Bates, A.; Ducarme, V.; Mirodatos, C. Oxidative Conversion of Methane and C_2 Hydrocarbons on Oxides: Homogeneous versus Heterogeneous Processes. *Appl. Catal.* **1989**, *47*, 287.

McCarty, J. G. Mechanism of Cooxidative Methane Dimerization Catalysis: Kinetic and Thermodynamic Aspects. in *Methane conversion by oxidative processes*; Wolf, E. E., Ed.; Van Nostrand Reinhold: New York, 1992; p 320.

Mears, D. E. Diagnostic Criteria for Heat Transport Limitations in Fixed Bed Reactors. *J. Catal.* **1971**, *20*, 127.

Meixner, D. L.; Arthur, D. A.; George, S. M. Kinetics of Desorption, Adsorption and Surface Diffusion of CO_2 on MgO(100). *Surf. Sci.* **1992**, *261*, 141.

Nibbelke, R. H.; Scheerová, J.; de Croon, M. H. J. M.; Marin, G. B. The Oxidative Coupling of Methane over MgO Based Catalysts: a Steady State Isotope Transient Kinetic Analysis. *J. Catal.* **1995**, *156*, 106.

Peil, K. P.; Goodwin, J. G.; Marcelin, G. An Examination of the Oxygen Pathways during Methane Oxidation over a Li/MgO Catalyst. *J. Phys. Chem.* **1989**, *93*, 5977.

Polyakov, M. V.; Stadnik, P. M.; Neimark, I. E. Heterogeneous−homogeneous catalysis of CH_4+O_2 mixtures. *Zh. Fiz. Khim.* **1936**, *8* (4), 584.

Reyes, S. C.; Iglesia, E.; Kelkar, C. P. Kinetic Transport Models of Bimodal Reaction Sequences-I. Homogeneous and Heterogeneous Pathways in Oxidative Coupling of Methane. *Chem. Eng. Sci.* **1993**, *48* (14), 2643.

Roos, J. A.; Korf, S. J.; Veehof, R. H. J. van Ommen, J. G.; Ross, J. R. H. Kinetic and Mechanistic Aspects of the Oxidative Coupling of Methane over a Li/MgO Catalyst. *Appl. Catal.* **1989**, *52*, 131.

Sanches-Marcano, J.; Mirodatos, C.; Wolf, E. E.; Martin, G. A. Inhibition of Gas-Phase Oxidation of Ethylene by Various Solids and Influence of Their Addition on the Catalytic Properties of Lanthanum Oxide Towards the Oxidative Coupling of Methane. *Catal. Today* **1992**, *13*, 227.

Shi, C.; Hatano, M.; Lunsford, J. H. A Kinetic Model for the Oxidative Coupling of Methane over Li_+MgO catalysts. *Catal. Today* **1992**, *13*, 191.

Sinev, M. Y. Elementary Steps of Radical−Surface Interactions in Oxidative Coupling of Methane. *Catal. Today* **1992**, *13*, 561.

Sinev, M. Y.; Korchak, V. N.; Krylov, O. V. 1988, Mechanism of Oxidative Condensation of Methane into C_2 Hydrocarbons over Oxide Catalysts. In *Proceedings of the 9th International Congress on Catalysis*; Vol. 2, Phillips, M. J., Ternan, M., Eds.; 968−973, The Chemical Institute of Canada: Ottawa, Canada, 1988; Vol. 1, pp 968−973.

Smith, K. J.; Galuszka, J. Effect of CO_2 on Methane Oxidative Coupling Kinetics. *Ind. Eng. Chem. Res.* **1994**, *33* (1), 14.

Temkin, M. I. The Kinetics of Steady-State Complex Reactions. *Int. Chem. Eng.* **1971**, *11* (4), 709.

Tong, Y.; Lunsford, J. H. Mechanistic and Kinetic Studies of the Reactions of Gas-Phase Methyl Radicals with Metal Oxides. *J. Am. Chem. Soc.* **1991**, *113*, 4741.

Tulenin, Y.; Kadushin, A.; Seleznev, V.; Shestakov, A.; Korchak, V. Effect of Pressure on the Process of Methane Oxidative Dimerization. Part 1. The Mechanism of Heterogeneous Inhibition of the Gas Phase Reactions. *Catal. Today* **1992**, *13*, 329.

Tung, W.-Y.; Lobban, L. L. Oxidative Coupling of Methane over Li/MgO: Kinetics and Mechanism. *Ind. Eng. Chem. Res.* **1992**, *31*, 1621.

van der Wiele, K.; Geerts, J. W. H. M.; van Kasteren, J. M. N. Elementary Reactions and Kinetic Modeling of the Oxidative Coupling of Methane. In *Methane conversion by oxidative processes*; Wolf, E. E., Ed.; Van Nostrand Reinhold: New York, 1992; p 259.

Zanthoff, H. W.; Baerns, M. Combined Kinetics of Catalytic and Non-Catalytic Reactions in the Oxidative Coupling of Methane. Preprints for ACS Symposium on Natural Gas Upgrading, San Francisco, April, 1992.

Zdanov, V. P.; Pavlicek, J.; Knor, Z. Pre-exponential Factors for Elementary Surface Processes. *Catal. Rev., Sci. Eng.* **1988**, *30*, 501.

Received for review July 25, 1995
Revised manuscript received June 24, 1996
Accepted June 24, 1996[⊗]

IE9504617

[⊗] Abstract published in *Advance ACS Abstracts,* August 15, 1996.